Supporting Information

Assmy et al. 10.1073/pnas.1309345110

SI Materials and Methods

Site Selection, Fertilization, and Tracking of the Fertilized Patch. The eddy was located, and its position during the experiment monitored, in satellite images of sea-surface height (http://argo.colorado.edu/~realtime/gsfc_global-real-time_ssh/). The patch was fertilized by releasing $7*10^3$ kg of dissolved ferrous sulfate in concentric circles around a drifting buoy to yield a concentration of 1.5 nmol·L^{-1} on day 0. Two weeks later, another $7*10^3$ kg of $FeSO_4$ was added to the spreading patch equivalent to 0.34 nmol·L^{-1}. The movement of the center of the fertilized patch was tracked by a surface buoy drogued at 18- to 26-m depth, equipped with Global Positioning System receivers and radio as well as ARGOS satellite transmitters. The patch was located with the drifting buoy and by continuous, underway measurements of the photochemical efficiency (Fv/Fm). Within a week, the bloom had accumulated sufficient biomass so that additional tracers (chlorophyll and online fCO_2 concentrations) were used to locate the part of the patch least affected by dilution with outside water, i.e., with the highest chlorophyll and, in the last week, the lowest fCO_2 concentration. All in-stations were placed inside this "hot spot," and care was taken to locate it with small-scale surveys before sampling and to keep the ship within it during the stations, which generally lasted about 8 h (1). Some in-stations and casts, although within the patch but subsequently shown to have missed the hot spot, have been excluded. The control "out-stations" were taken within the eddy core well away from the patch but (for logistical reasons) in different locations relative to it. The first station (day −1) was sampled 1 d before iron addition and can be considered as representative of initial conditions for both in- and out-patch stations. In-patch stations always sampled the same water mass; casts taken when the ship inadvertently drifted out of the hot spot were discarded. Out-patch stations were located in different water columns relative to the patch but nevertheless provided a coherent picture of processes in unfertilized water. Vertical coherence of the deep-water column with its respective surface layer was demonstrated by the trajectories of four autonomous APEX (Autonomous Profiling Explorer; Webb Research) floats positioned between 200- and 1,000-m depth over a 2-wk period extending beyond the end of the experiment and by different models based on hydrography and altimeter images. Details are presented elsewhere (1).

Biological Bulk Properties. Sampling was carried out with Niskin bottles mounted on a CTD rosette equipped with a profiling transmissometer. Particulate organic carbon (POC), nitrogen (PON), biogenic silica (BSi), chlorophyll *a* (Chl *a*), and primary production were analyzed using standard protocols (1). Inorganic nutrients (silicate, phosphate, nitrate, nitrite, and ammonium) were measured with a Technicon AutoAnalyzer II system using standard methods. Photosynthetic efficiency (Fv/Fm) was measured online with a fast repetition rate fluorometer. Pigment analyses were performed by HPLC according to (2). Colorimetric measurements of transparent exopolymer particles (TEPs) were performed as described by Passow and Alldredge (3). For TEP microscopy, formalin-fixed plankton samples were filtered onto 0.4-μm Nuclepore Track Etch Membranes (Whatman), stained with Alcian blue, and fixed on CytoClear slides (Osmonics) according to Logan et al. (4).

Plankton Sampling and Quantification. ***Water samples.*** For the qualitative and quantitative assessment of the plankton assemblage, duplicate 200-mL water samples were obtained from Niskin bottles from seven discrete depths between 10 and 150 m at the initial station and at eight in- and four out-patch stations. Plankton samples were taken from the same cast together with all core parameters (Chl *a*, nutrients, pCO_2, POC, PON, and BSi). One set of samples was preserved with hexamethylenetetramine-buffered formaldehyde solution and one with Lugol's iodine at a final concentration of 2% and 5% (vol/vol), respectively. Fixed samples were stored at 4 °C in the dark until counting back in the home laboratory. Diatoms and other protists with robust cell walls were enumerated in hexamethylenetetramine-buffered formaldehyde-fixed samples, whereas unarmored species (athecate dinoflagellates, aloricate ciliates, and flagellates) were counted in Lugol's iodine solution. Cells were identified and enumerated using inverted light and epifluorescence microscopy (Axiovert 25 and Axiovert 135; Zeiss) as described by Throndsen (5). Subsamples were settled in 50-mL sedimentation chambers (Hydrobios) for 48 h. Each sample was examined until at least 500 cells had been counted. Uncertainties in cell abundance were estimated assuming a random distribution of cells in the counting chambers (6).

To acquire information on species-specific diatom mortality, whole intact empty and recognizable broken frustules were counted in addition to full cells. Only broken diatom frustules of which >50% of the frustule was recognizable were considered. In the case of *Thalassiothrix antarctica*, only broken ends with apical spines, present at only one end, were counted. As the girdle, composed of numerous small scale-like bands, of *Proboscia* and *Rhizosolenia* species rapidly disintegrates upon cell death, only epivalves and hypovalves with signs of damage were considered. Empty and broken frustules were identified to species or genus level and otherwise grouped into size classes. Empty diatom frustules are easy to recognize and identify, and hence provide valuable information on the incidence of cell mortality in species populations (7). Mortality can be due to a broad range of mechanisms such as (*i*) death due to viral, bacterial, or parasitoid infection, (*ii*) ingestion and digestion of cell contents by protozoa (including pallium-feeding dinoflagellates), and metazooplankton such as salps (copepods and euphausiids damage most, but not all, of the ingested diatoms), (*iii*) cell death due to unfavorable environmental conditions such as light deprivation or nutrient limitation, (*iv*) internal regulation of mortality by mechanisms such as cell lysis and/or apoptosis (programmed cell death), and (*v*) gametogenesis in sexual phases when gametes, and later the zygote, abandon the frustule. Broken frustules are due to crustacean (mainly copepods) biting with or without ingestion. Estimates of mortality rates from the ratios of full to empty and broken frustules are dependent on their robustness and size. Thus, the percentage of frustules crushed beyond recognition varies between species and grazer. For instance, robust frustules such as those of *Fragilariopsis kerguelensis* are likely to withstand damage by smaller copepods better than those of *Pseudo-nitzschia*, which again will perform better than those of *Chaetoceros debilis*. The long, thick-walled frustules of *Thalassiothrix antarctica*, even if broken into small pieces, will hardly escape detection. At the other extreme are small, thin-walled diatom species whose frustule remains can no longer be quantified under light microscopy. Therefore, the high ratios of full and empty to broken frustules (~10:1) of large, conspicuous, needle-shaped species, in particular *T. antarctica* and *Proboscia alata*, recorded throughout the experiment are proof that these species are avoided by copepod grazers in surface and subsurface layers.

For prokaryotic abundance, 10–20 mL of water samples were fixed with 3% (vol/vol) formaldehyde (final concentration), stained with DAPI, and filtered onto 0.2-μm, black polycarbonate filters. DAPI-stained cells collected on the filters were enumerated on a Zeiss Axioplan 2 microscope equipped with a 100-W Hg lamp and appropriate filter sets for DAPI. Prokaryotic abundance was converted to prokaryotic carbon biomass using the factor 20 fg C·cell^{-1} (8).

Concentrated samples. An extra CTD cast was sampled for the assessment of larger and less abundant protozoa (radiolaria, acantharia, foraminifera, and heliozoa), large *Phaeocystis antarctica* colonies, fecal pellets, as well as copepods <1 mm (including nauplii, copepodites, and adults of small copepod species). The whole content of one to two Niskin bottles (12–24 L) was concentrated to 50 mL by gently pouring the water through a 20-μm mesh net. Samples were taken at 11 depths between 10 and 350 m at the initial station and at seven in- and four out-patch stations. These samples were supersaturated with strontium chloride to prevent the dissolution of the acantharian skeletons (9).

To follow the sinking of the bloom through the deeper layer of the water column, diatoms as well as other microplankton species were enumerated in concentrated samples from 200-, 250-, 300-, and 350-m depth and two deep CTD casts down to the seafloor on day 36 inside and day 34 outside the patch. Sampling depths in the deep casts were chosen according to the number and magnitude of spikes in the transmissometer profile. In case of the deep samples, the content of one Niskin bottle (12 L) was concentrated down to 50 mL by pouring the water gently through a 10-μm mesh net. Special care was taken not to contaminate the deep samples with surface water by thoroughly washing the nets and tubes with fresh water after each sample collection. All concentrated samples were fixed with hexamethylenetetramine-buffered formaldehyde solution at a final concentration of 2% (vol/vol) and stored at 4 °C in the dark.

Multi-Net samples. For the qualitative and quantitative estimation of copepods >1 mm, the water column down to 400 m was sampled at five standard depths (25, 50, 100, 160, and 400 m) with a Multi-Net (55- and 100-μm mesh size) on a regular basis inside and outside the fertilized patch during night and day. For later identification and counting, samples were fixed with hexamethylenetetramine-buffered formaldehyde solution at a final concentration of 4% (vol/vol). Several individuals of the most abundant copepods >1 mm from in-patch and out-patch stations were carefully caught with Bongo nets, kept in 0.2-μm filtered seawater for 24 h at 4 °C, and subsequently deep-frozen at −20 and −80 °C for carbon analysis.

Estimation of Carbon Content, Depth Integrated Stocks, and Accumulation Rates. In case of phytoplankton and microzooplankton, at least 10–30 randomly chosen individuals of each species were measured and the average cell size was used to calculate the biovolume from equivalent geometrical shapes (10). The biovolume was converted to cellular carbon content through carbon conversion equations recommended by Menden-Deuer and Lessard (11). The biovolume of empty and broken frustules was also calculated and converted into carbon equivalents for a better comparison with full frustule biomass and BSi standing stocks. Tintinnid cell biomass was calculated as for other ciliates. Because of the large size differences in this group, stocks of empty intact and damaged loricae were converted into species-specific biomass equivalents for direct comparison with loricae containing ciliates (full loricae). In case of foraminifera, the biovolume was determined by assuming a spherical shape and using the longest dimension across the calcite test as the diameter (12). Biovolumes of acantharia were calculated assuming a sphere, or a spheroid shape (13). For adult radiolaria, biovolume was measured as the diameter of the spherical central capsule (13). Biovolumes were converted to biomass using measured carbon/volume ratio estimates (0.08 mg·mm^{-3} for acantharia, 0.089 mg·mm^{-3} for foraminifera, and 0.01 mg·mm^{-3} for radiolaria and heliozoa) according to ref. 13. The carbon content of the *Phaeocystis* colony skin was estimated using the following relationship: nanograms C colony = 213 × (colony volume in cubic millimeters) (14). At least 30 randomly chosen nauplii of each of the three major copepod taxa present in the samples (calanoid, cyclopoid, and harpacticoid species) were measured to determine the average body volume, which was multiplied by 0.08 to obtain the carbon content (15). The carbon content of copepods <1 and >1 mm was directly estimated from C/N analysis (Carlo Erba NA-1500 Analyzer) of picked individuals according to refs. 15 and 16. Fecal pellet volume (FPV) and fecal pellet carbon (FPC) were calculated using recommended geometrical shapes (11) and a carbon conversion factor of 0.07 mg C·mm^{-3} (17), respectively. Fecal pellets were counted in the following categories: complete, broken with one end missing, or highly fragmented.

The data on particle stocks and species populations of each station are presented as biomass (carbon per square meter) derived from trapezoidal depth integration of measurements carried out on six to nine discrete water samples taken from standard depths at 10- to 20-m intervals in the 100-m mixed layer, 50-m intervals in the 200- to 350-m depth layer and larger intervals for the deep-water column down to the seafloor.

Accumulation rates, i.e., the difference between growth and mortality rates, were calculated by estimating the slope of the regression for the log-transformed values of cell concentrations over the time interval in which exponential increase was recorded. Corrections for dilution due to spreading of the patch are described in ref. 1.

Statistics Applied to Subsurface Layer Data Presented in Fig. 3. We applied a one-sample, one-sided t test to ascertain whether the differences in sinking behavior of *Chaetoceros dichaeta*, *Fragilariopsis kerguelensis*, and *Thalassiothrix antarctica* between IN and OUT stations for the subsurface layer (SSL) from 200- to 350-m depth are statistically significant (Table S1). We tested the working hypothesis $\Delta c > 0$ ("higher concentrations at IN stations") against the null hypothesis $\Delta c < 0$ ("lower concentrations at IN stations"). We calculated $\Delta c = c_{IN} - c_{OUT}$, where c_{IN} and c_{OUT} are the biomass concentrations (micrograms of carbon per liter) in case of full cells and abundances (frustules per liter) in case of intact empty and broken frustules inside and outside the patch, respectively. By pooling the Δc values over the SSL, we obtained a statistical sample with a sample size $n = 4$. Out-patch days 26 and 34 (since first iron addition) were compared with the respective preceding and subsequent in-patch days. All but one null hypotheses could be rejected on the traditional evidence level $\alpha = 0.05$ and on the evidence level $\alpha = 0.1$ for *C. dichaeta* but not for *F. kerguelensis*. Given the small sample size ($n = 4$) and the sampling time differences between in-patch and out-patch stations, one has to expect quite a bit of statistical noise. However, it needs to be noted that the P values for *F. kerguelensis* were almost always higher, particularly in the case of empty and broken frustules, than those for *C. dichaeta* over corresponding time intervals, showing that frustules of *F. kerguelensis* continuously sank out of the surface layer irrespective of the iron status. In contrast, concentrations of full, empty, and broken C. *dichaeta* were much larger under the patch than outside the patch during the peak of the flux event (IN day 32 versus OUT day 34) as illustrated by the very low P values. The scatter in P values for *T. antarctica* are expected given the very low presence of this species in SSL.

Carbon Ingestion Rates Estimated from Fecal Pellet Production Experiments. Fecal pellet production was estimated from experiments conducted with four dominant calanoid copepod species

(*Calanus simillimus*, *Rhincalanus gigas*, *Pleuromamma robusta*, and *Calanus propinquus*) and by allometric scaling to estimate fecal pellet production of juvenile stages and the small species *Ctenocalanus citer*. Experiments were conducted at different in- and out-patch stations over the course of the European Iron Fertilization Experiment (EIFEX). Two to four—depending on the size of the species—healthy, adult females were retrieved from Bongo net catches and transferred into three to five parallel 1- or 2-L incubation bottles containing mixed-layer water collected at the station. Bottles were placed on a slowly rotating plankton wheel at in situ temperature and dim light. After 24 h of grazing on the natural plankton community, the content of the bottles was carefully sieved over 30-μm plankton mesh and fixed with hexamine-buffered formaldehyde [4% (vol/vol) final concentration] for later enumeration and size measurements of fecal pellets. Fecal pellet production estimates from the bottle experiments were multiplied by the abundances of the respective species recorded in the upper 160 m, to obtain total daily carbon ingestion in the field. Respiratory needs were added to the fecal pellet production estimates to account for total carbon ingestion. Copepod respiration was assumed to equal 6.5% of the copepod carbon standing stock per day (18).

Because no copepod biomass data were available for out-station 514 (day 17), the standing stocks from out-station 509 (day 11) were used to calculate the respiratory needs. The daily carbon ingestion by copepods increased fivefold from 0.2 to 1 g $C{\cdot}m^{-2}{\cdot}d^{-1}$, which amounted in total to 20 g $C{\cdot}m^{-2}$ over the course of EIFEX (15 g $C{\cdot}m^{-2}$ for fecal pellet production and 5 g $C{\cdot}m^{-2}$ for respiratory needs, respectively).

Carbon Ingestion Rates Estimated from Gut Evacuation Experiments. Gut evacuation experiments were conducted with abundant copepod species collected inside and outside the fertilized patch with a Bongo net during night and day. The Bongo net (100 and 300 μm) was towed vertically from depths between 150 and 20 m to the surface—depending on the time of day—at a maximum speed of 0.3 $m{\cdot}s^{-1}$. After retrieval of the net, the content of the cod end was immediately transferred into a cooler with 20 L GF/F filtered seawater at in situ temperature. Still on deck, subsamples were retrieved from the diluted catch on a piece of fine mesh for determination of the initial gut pigment content (G0). The mesh was packed in aluminum foil and shock frozen at −80 °C. For estimating of gut evacuation rate, a time series of subsequent samples was collected typically after 1, 2, 4, 6, 10, 20, and 30 min. Frozen samples were thawed on board and copepods sorted in a cooled Petri dish under a stereomicroscope at dim light. One to 20 individuals for each species were placed in a 20-mL PE centrifuge vial, covered with 5 mL of 90% (vol/vol) aqueous acetone, and left in a refrigerator for extraction of pigments for 24 h. Pigment concentration was measured with a Turner fluorometer before and after acidification. A correction factor for pigment destruction to nonfluorescent components was included by multiplying the concentration of phaeopigments by 1.5. Calculation of the gut clearance coefficient, k, and the gut passage time (GPT), was based on the exponential model of ref. 19:

$$k = (\ln(\mathrm{G0}) - \ln(\mathrm{G}(t)))/t$$
$$\mathrm{GPT} = 1/k,$$

where G0 represents the initial gut content (nanograms of pigment per individual), and G(t), the gut content at a given time t. The quotient of $1/k$ represents the GPT in minutes. Daily ingestion (nanograms of pigment per individual per day) is derived from initial gut content G0 and k according to the equation:

$$\mathrm{I} = \mathrm{G0} \times k \times 60 \times 12.$$

A grazing period of 12 h was assumed to account for the observed periodicity in the migration and likely feeding behavior of the copepods. Ingestion rates were obtained by multiplying the initial gut content with the respective gut clearance rate that was experimentally determined. Pigment concentrations were converted to phytoplankton carbon (PPC) using a C:Chl *a* ratio of 30. For estimation of the grazing rates, PPC ingestion was related to copepod carbon weight and expressed as percentage of body carbon ingested per day (daily ration).

Constant daily rations for the different species were based on findings during this (EIFEX) and a previous iron fertilization experiment (20) as well as on additional literature values (21–24).

1. Smetacek V, et al. (2012) Deep carbon export from a Southern Ocean iron-fertilized diatom bloom. *Nature* 487(7407):313–319.
2. Hoffmann L, Peeken I, Lochte K, Assmy P, Veldhuis M (2006) Different reactions of Southern Ocean phytoplankton size classes to iron fertilization. *Limnol Oceanogr* 51(3):1217–1229.
3. Passow U, Alldredge AL (1995) A dye-binding assay for the spectrophotometric measurement of transparent exopolymer particles (TEP). *Limnol Oceanogr* 40(7): 1326–1335.
4. Logan BE, Grossart H-P, Simon M (1994) Direct observation of phytoplankton, TEP, and aggregates on polycarbonate filters using brightfield microscopy. *J Plankton Res* 16(12):1811–1815.
5. Throndsen J (1995) Estimating cell numbers. *Manual on Harmful Marine Microalgae*, eds Hallegraeff GM, Anderson DM, Cembella AD (UNESCO, Paris), pp 63–80.
6. Zar JH (2010) *Biostatistical Analysis* (Prentice Hall International, London), 5th Ed.
7. Assmy P, Henjes J, Klaas C, Smetacek V (2007) Mechanisms determining species dominance in a phytoplankton bloom induced by the iron fertilization experiment EisenEx in the Southern Ocean. *Deep Sea Res Part I Oceanogr Res Pap* 54(3):340–362.
8. Lee S, Fuhrman JA (1987) Relationships between biovolume and biomass of naturally derived marine bacterioplankton. *Appl Environ Microbiol* 53(6):1298–1303.
9. Beers JR, Stewart GL (1970) The preservation of Acantharians in fixed plankton samples. *Limnol Oceanogr* 15(5):825–827.
10. Hillebrand H, Duerselen CD, Kirschtel D, Pollingher U, Zohary T (1999) Biovolume calculation for pelagic and benthic microalgae. *J Phycol* 35(2):403–424.
11. Menden-Deuer S, Lessard EJ (2000) Carbon to volume relationships for dinoflagellates, diatoms and other protist plankton. *Limnol Oceanogr* 45(3):569–579.
12. Bé AWH, et al. (1977) Laboratory and field observations of living planktonic foraminifera. *Micropaleontology* 23(2):155–179.
13. Michaels AF, Caron DA, Swanberg NR, Howse FA, Michaels CM (1995) Planktonic sarcodines (Acantharia, Radiolaria, Foraminifera) in surface waters near Bermuda: Abundance, biomass and vertical flux. *J Plankton Res* 17(1):131–163.
14. Mathot S, et al. (2000) Carbon partitioning within *Phaeocystis antarctica* (Prymnesiophyceae) colonies in the Ross Sea, Antarctica. *J Phycol* 36(6):1049–1056.
15. Postel L, Fock H, Hagen W (2000) Biomass and abundance. *ICES Zooplankton Methodology Manual*, eds Harris RP, Wiebe PH, Lenz J, Skjodal HR, Huntley M (Academic, London), pp 83–191.
16. Meyer B, Atkinson A, Blume B, Bathmann UV (2003) Feeding and energy budgets of larval Antarctic krill *Euphausia superba* in summer. *Mar Ecol Prog Ser* 257:167–177.
17. Riebesell U, Reigstad M, Wassmann P, Noji T, Passow U (1995) On the trophic fate of *Phaeocystis pouchetii* (Hariot): 6. Significance of *Phaeocystis*-derived mucus for vertical flux. *Neth J Sea Res* 33(2):193–203.
18. Dagg MJ, Vidal J, Whitledge TE, Iverson RL, Goering JJ (1982) The feeding, respiration, and excretion of zooplankton in the Bering Sea during a spring bloom. *Deep Sea Res* 29(1):45–63.
19. Dam HG, Peterson WT (1988) The effect of temperature on the gut clearance rate constant of planktonic copepods. *J Exp Mar Biol Ecol* 123(1):1–14.
20. Schultes S (2004) The role of zooplankton grazing in the biogeochemical cycle of silicon in the Southern Ocean. PhD thesis (Univ of Bremen, Bremen, Germany).
21. Mayzaud P, et al. (2002) Carbon intake by zooplankton. Importance and role of zooplankton grazing in the Indian sector of the Southern Ocean. *Deep Sea Res Part II Top Stud Oceanogr* 49(16):3169–3187.
22. Dubischar CD, Bathmann UV (1997) Grazing impact of copepods and salps on phytoplankton in the Atlantic sector of the Southern Ocean. *Deep Sea Res Part II Top Stud Oceanogr* 44(1-2):415–433.
23. Atkinson A, Ward P, Murphy EJ (1996) Diel periodicity of Subantarctic copepods: Relationships between vertical migration, gut fullness and gut evacuation rate. *J Plankton Res* 18(8):1387–1405.
24. Schnack-Schiel SB, Hagen W, Mizdalski E (1991) Seasonal comparison of *Calanoides acutus* and *Calanus propincuus* (copepoda: Calanoida) in the south-eastern Weddel Sea, Antarctica. *Mar Ecol Prog Ser* 70:17–27.

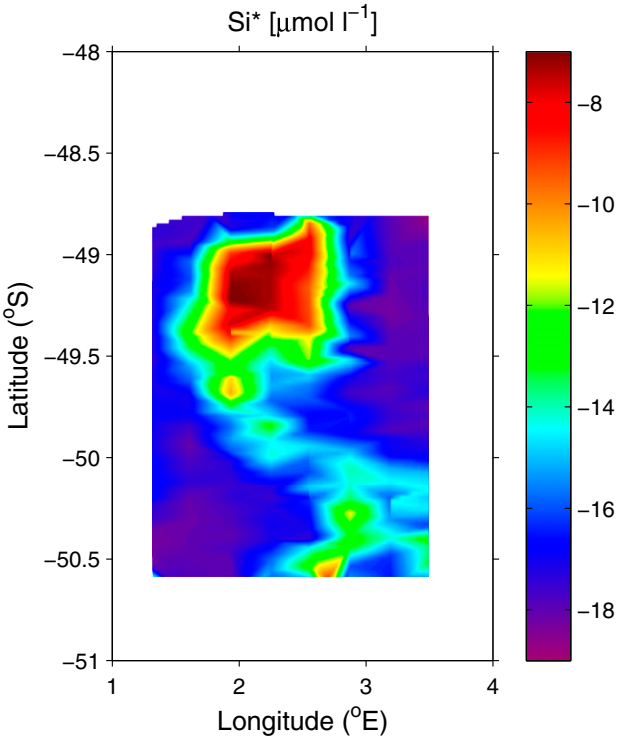

Fig. S1. Distribution of Si* during the eddy survey carried out from day 1 to day 7 after fertilization showing clear distinction between the eddy core (the orange/red area) and the surrounding frontal meander.

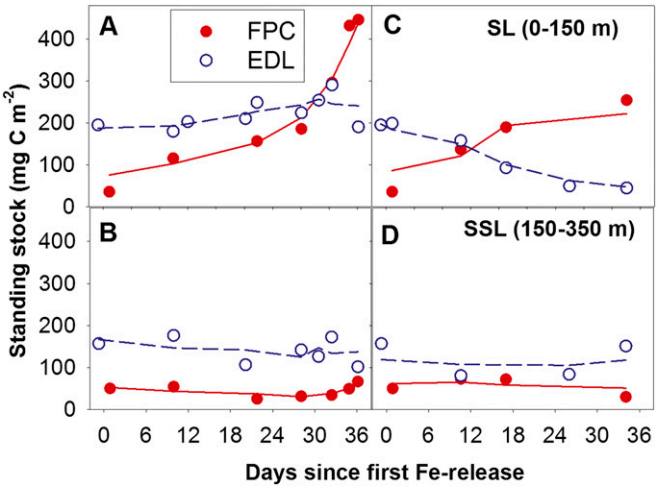

Fig. S2. Standing stocks of copepod fecal pellet carbon and carbon equivalents of empty and damaged tintinnid loricae. Copepod fecal pellet carbon (FPC) stocks (the sum of whole pellets and fragments) (filled red circles) and the sum of empty and damaged tintinnid loricae (EDL) presented as equivalent biomass values (open blue circles) integrated for the surface layer (SL: 0–150 m) and the subsurface layer (SSL: 150–350 m) inside (*A* and *B*) and outside (*C* and *D*) the patch. The lines represent the running average for FPC (solid line) and EDL (dashed line) stocks. Note low pellet stocks in the SSL compared with the surface. We conclude from the difference in stock sizes between SL and SSL and the estimated residence time of pellets in the SL of 24 h that the bulk of pellets produced in the SL was retained there by fragmentation and ingestion. Indeed, generally >80% of all fecal pellets counted were either missing one end or were highly fragmented throughout the upper 550 m of the water column. In contrast, stock sizes of tintinnid loricae, with comparable sinking rates as pellet fragments, are similar in upper and lower layers presumably because of their greater durability. Whole, but often damaged, tintinnid loricae were frequently seen in copepod fecal pellets. Apparently, their leathery consistency (they are also made of proteins) prevent their crushing into small pieces by copepod gnathosomes.

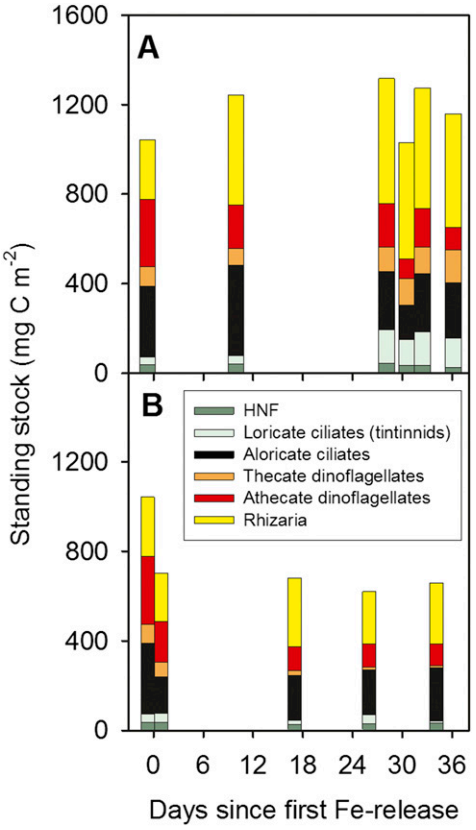

Fig. S3. Protozooplankton standing stocks. Protozooplankton standing stocks inside (*A*) and outside (*B*) the patch with contributions of heterotrophic nanoflagellates (HNF), loricate (tintinnid), and aloricate (naked) ciliates (only full loricae were considered in the former), thecate (armored) and athecate (naked) aplastidic dinoflagellates, and Rhizaria (including acantharia, foraminifera, radiolaria, and heliozoa). Note that, despite species succession within each component, their total biomass (with the exception of Rhizaria) did not change significantly during the experiment, which we attribute to heavy grazing pressure exerted by the large copepod community, exemplified by the tintinnids in Fig. 3. Outside the patch, total biomass declined as in the case of all other protistan plankton. Within the Rhizaria, the bulk of the doubling of biomass inside the patch was due to acantharia, a group characterized by numerous outward-pointing, sharp spines made of strontium sulfate. We believe that the large, strong spines provide protection against ingestion by copepods as adult acantharia, although highly conspicuous, were rarely seen in fecal pellets. We conclude that, as in the case of diatoms, low mortality rather than fast growth rates compared with other protists, were the main cause of their increase.

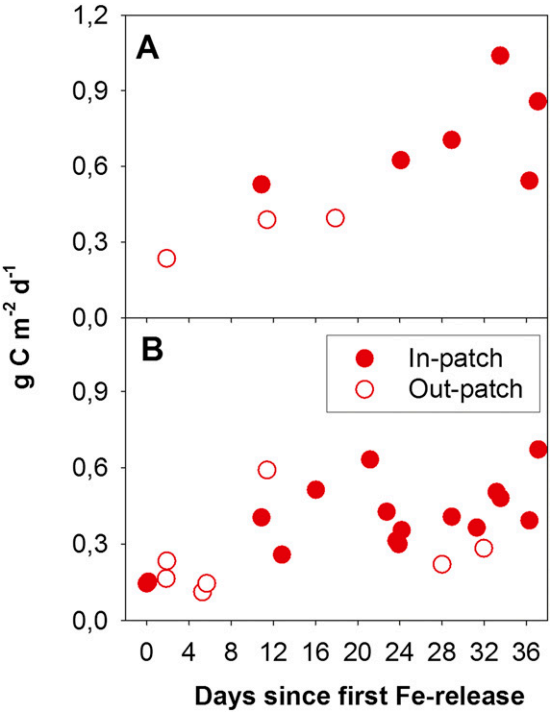

Fig. S4. Copepod grazing estimates. (*A*) Total carbon ingestion derived from fecal pellet carbon production experiments, corrected for respiratory needs, of dominant copepod species over the course of EIFEX. (*B*) Phytoplankton carbon (PPC) ingestion rates estimated from copepod gut evacuation experiments over the course of EIFEX. Our grazing estimates are in the same range as those reported from the APF during spring and summer (1, 2).

1. Mayzaud P, et al. (2002) Carbon intake by zooplankton. Importance and role of zooplankton grazing in the Indian sector of the Southern Ocean. *Deep Sea Res Part II Top Stud Oceanogr* 49(16):3169–3187.
2. Urban-Rich J, Dagg M, Peterson J (2001) Copepod grazing on phytoplankton in the Pacific sector of the Antarctic Polar Front. *Deep Sea Res Part II Top Stud Oceanogr* 48(19-20):4223–4246.

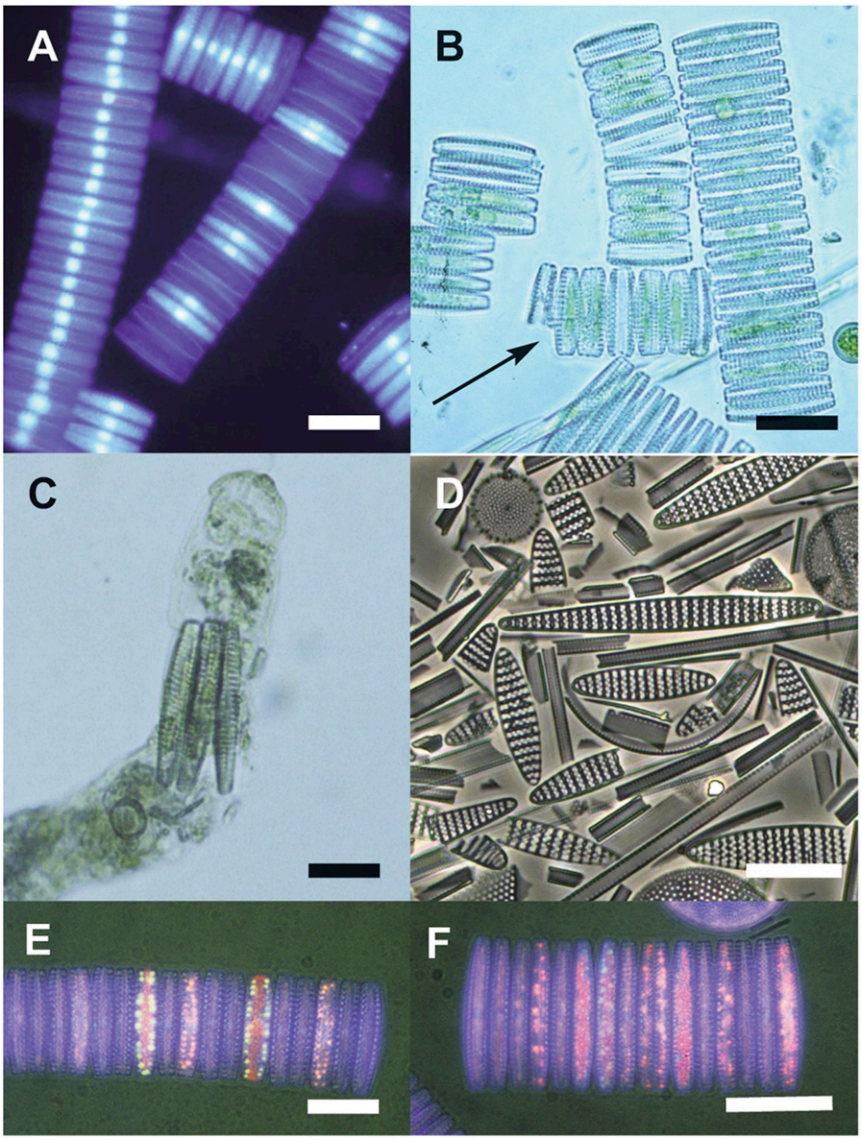

Fig. S5. Micrographs of the silica-sinking diatom *Fragilariopsis kerguelensis* collected from field samples. (*A*) Two long chains with nuclei stained with DAPI (a DNA dye) showing numerous empty, intact frustules in one chain. (Scale bar: 50 μm.) (*B*) Intact chains with single bitten terminal cells (marked by arrows) indicate rejection by the copepod after a sampling bout. (Scale bar: 50 μm.) (*C*) Three intact cells inside a copepod fecal pellet. (Scale bar: 30 μm.) Copepods feed sparingly on this species presumably because they are deterred by the energy expenditure and wearing of mandibular teeth associated with crushing the strong frustules, which also increase gut fullness. (*D*) Antarctic sediment sample characteristic of the iron-limited southern Antarctic Circumpolar Current showing dominance of empty, intact valves. (*E* and *F*) Two chains stained with the lipid dye Nile Red showing differentiation of cells within the same chain reflected in large variation in lipid content, implying greater viability in cells with oil droplets. Apoptosis of weaker cells could account for the empty frustules in *A*. Indeed, the cells in a diatom chain are not necessarily identical in terms of viability (1). (Scale bar: 50 μm.)

1. Laney SR, Olson RJ, Sosik HM (2012) Diatoms favor their younger daughters. *Limnol Oceanogr* 57(5):1572–1578.

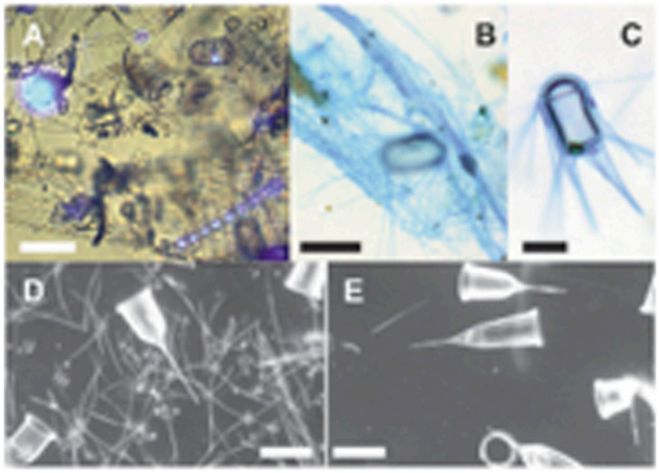

Fig. S6. Light micrographs of phytoplankton aggregates from 300-m depth under the patch. (*A*) Portion of a 4-mm-long aggregate stained with DAPI (DNA dye) comprising empty and full (with blue nuclei) cells and chains of *Chaetoceros* spp. embedded in a sticky, mucoid matrix. (Scale bar: 100 μm.) (*B*) Empty frustules of *Chaetoceros atlanticus* and *Corethron pennatum* entangled in a mucoid sheath weakly stained by Alcian blue specific for acidic polysaccharides. (Scale bar: 50 μm.) (*C*) Cell of *C. pennatum* oozing out its autolysed, Alcian blue-stained cytoplasm, which has stuck the rigid spines into bundles. (Scale bar: 50 μm.) Multi-Net samples (100-μm mesh) from the layer 160–400 m showing mass presence of *Chaetoceros* spp. under the patch (*D*) during the flux event and absence outside it (*E*). In contrast, empty and damaged tintinnid loricae of *Cymatocylis* spp. are present both underneath the patch and outside it. (Scale bars: 100 μm.)

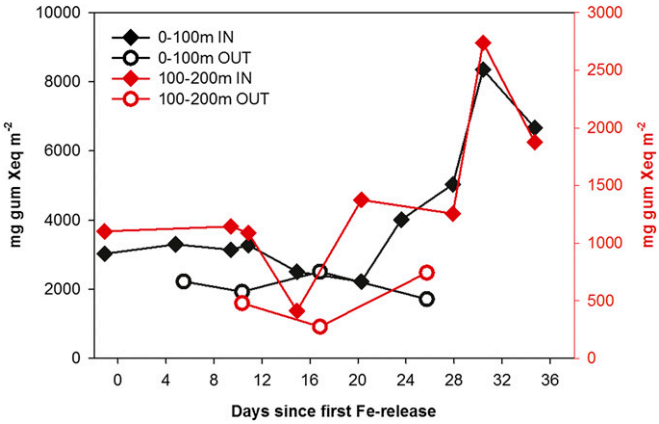

Fig. S7. Transparent exopolymer particles (TEPs). Temporal development of TEPs in gum Xanthan equivalents per square meter for the surface layer (0–100 m, black lines and scale) and the subsurface layer (100–200 m, red lines and scale) inside and outside the fertilized patch. Note the strong increase in TEPs during the flux event inside and under the patch.

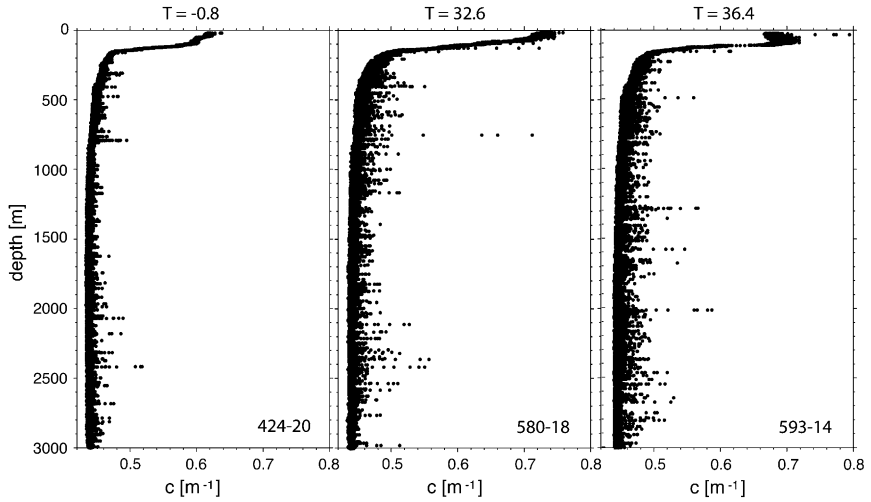

Fig. S8. Light beam attenuation profiles for the upper 3,000 m of the water column recorded by the transmissometer under the hot spot before fertilization (day −0.8) and during the flux event on days 32.6 and 36.4. Note the increase in spikes throughout the water column in the end phase of the experiment.

Table S1. One-sample, one-sided *t* test applied to subsurface layer data presented in Fig. 3

Species	IN day	OUT day	*P* value Full cells	*P* value Empty frustules	*P* value Broken frustules
C. dichaeta	20	26	0.058	0.015	0.058
	28	26	0.062	0.023	0.044
	32	34	0.0042	0.0083	0.0019
	36	34	0.031	0.060	0.26
F. kerguelensis	20	26	0.23	0.87	0.70
	28	26	0.048	0.39	0.31
	32	34	0.23	0.92	0.94
	36	34	0.047	0.032	0.95
T. antarctica	20	26	0.037	0.67	0.096
	28	26	0.086	0.11	0.033
	32	34	0.033	0.018	0.15
	36	34	0.098	0.020	0.44

Observed evidence levels (*P* values) for in-patch versus out-patch differences in full cells and empty and broken frustules of *Chaetoceros dichaeta*, *Fragilariopsis kerguelensis*, and *Thalassiothrix antarctica* for the subsurface layer (200–350 m). We have marked *P* values <0.05, <0.1, and >0.1 in red, blue, and black, respectively. For more information, see statistics in *SI Materials and Methods*. Sample size $n = 4$.